By acceptance of this article, the publisher or recipient acknowledges the U.S. Government's right to retain a non-exclusive, royalty-free license in and to any copyright covering the article.

CONF-761049--1

NOTICE
This report was prepared as an account of work sponsored by the United States Government. Neither the United States nor the United States Energy Research and Development Administration, nor any of their employees, nor any of their contractors, subcontractors, or their employees, makes any warranty, express or implied, or assumes any legal liability or responsibility for the accuracy, completeness or usefulness of any information, apparatus, product or process disclosed, or represents that its use would not infringe privately owned rights.

MODELS FOR IMPURITY PRODUCTION AND TRANSPORT IN TOKAMAKS*

J. T. Hogan
Oak Ridge National Laboratory
Oak Ridge, Tennessee 37830, USA

ABSTRACT

Models for the edge conditions which are commonly used in tokamak transport codes have been kept simple partly because of a lack of data. We present a report on an improved model for the particle and energy balance of e^-, H_1^+, H_1^o, H_2^+, H_2^o, O^o, $O^{(1\to 8)+}$ in the plasma scrape-off region. Experiments should yield the needed data in the near future, and allow us to test the model.

The diffusion of impurities has been studied with a neoclassical model. The role of 'anomalous spreading' of the impurity distribution has been studied for the case of Fe.. We present a model for the expulsion of low-Z (oxygen) impurities for cases where $q(0) > 1$, but in which a large shear-free region is produced in the plasma core.

1. INTRODUCTION

There are many computer models of tokamak transport (see the surveys by Mercier[1], Düchs[2], and Hogan[3]) Their treatment of edge effects has been kept relatively simple, in part because there is a scarcity of relevant data on many of the fundamental wall interaction processes. Typically, the edge values of plasma temperature and density in these codes will be held to some pre-determined value. The incoming fluxes of neutral gas and impurities are prescribed either by qualitative comparison with fast pressure measurements and line radiation intensities, or else they are chosen to satisfy some overall requirement on the temporal behavior. Examples of the latter are the condition of a fixed total number of particles, or an oxygen recycling rate equal to the hydrogen rate.

Because there are good prospects for a more detailed examination of some of the fundamental impurity production processes, we have improved the model used in the Oak Ridge Tokamak code to treat edge effects. We have been encouraged along these lines by the work presented by Hotson and McCracken[4]. Our boundary model is somewhat different, though, and it derives from the treatment of the C-Stellerator by Hinnov, Bishop, and Fallon[5]. These authors have modeled the entire stellerator discharge by solving coupled zero-dimensional rate equations for the time evolution of the energy and particle balance in a pure hydrogen plasma with a temperature around 10-50 eV. For our problem we construct a model for the time evolution of the energy and densities of electrons, H_1^+, H_1^o, H_2^+, H_2^o, O^o, $O^{(1\to 8)+}$ in the region of the tokamak which lies between the 'last flux surface,' i.e., that which touches the limiter, and the vacuum chamber wall. In Fig. 1 we show the generalized geometry. This edge plasma is characterized by the plasma surface area A_w and a mean thickness, Δ, defined such that the volume of plasma between the 'last flux surface' and the liner wall is $V_s = A_w \Delta$. We have chosen oxygen as the only impurity species in the edge plasma solely for simplicity. The wall chemistry is known to be much more complicated than this and to be imperfectly prescribed. This model is self-consistent, however, in that the production of neutral hydrogen and oxygen by charge exchange, photon and photoelectron desorption, plasma evaporation, thermodesorption and sputtering is calculated using outgoing fluxes provided by our radial transport model. The boundary conditions are then

*Research sponsored by the Energy Research and Development Administration under contract with Union Carbide Corporation.

NOTICE
PORTIONS OF THIS REPORT ARE ILLEGIBLE. It has been reproduced from the best available copy to permit the broadest possible availability.

MASTER

DISTRIBUTION OF THIS DOCUMENT IS UNLIMITED

determined by solving the correct particle and energy balance in the scrape-off region. These boundary conditions in turn provide the incoming neutral gas and impurity fluxes needed to describe the transport processes for the radial transport model.

The second part of this report on our ongoing work is devoted to a study of various impurity diffusion models. Since the needed data are poorly known for basic desorption and evaporation rates, and since the wall chemistry is complex and poorly known, we will use experimental measurements reported recently[6] to test the neoclassical impurity diffusion model. The cases of 'high-Z' (iron in our case) and 'low-Z' (oxygen) are presented separately.

In the first case we wish to see whether the measurement of central impurity densities provides an estimate of the 'anomalous spreading' which is commonly added to neoclassical impurity diffusion rates. Since we treat a low-current case, there is probably no significant charge exchange sputtering, so we ignore this source in the calculation.

In the second case, we examine the interplay between a large flux of oxygen ($\Psi_0 \sim 2 \cdot 10^{15}$ cm^{-2} s^{-1}) and the MHD stability of the tokamak. For a case where $q(0) > 1$ we find that fluxes of this magnitude can excite strong MHD activity by providing a core region of low shear. (This can also provide a mechanism for the strong disruptive instability[7] and would explain why the stability boundaries against disruption are narrowed when the vacuum vessel is poorly cleaned.) We will describe the model for boundary effects in Sect. 2. Section 3 describes the neoclassical diffusion studies of iron and oxygen.

2. BOUNDARY MODEL

We wish to consider the complex region between the 'last flux surface' and the vacuum chamber wall. The plasma (by which we shall mean the hot core plasma) is treated by the tokamak simulation model we describe in the Appendix. This model provides the sources or losses which drive the plasma/wall interaction from the plasma side; they are the processes we will treat in the model described here.

We will assume that the interface region carries no current and that the required electromagnetic properties are completely specified by providing the poloidal and toroidal magnetic fields.

The rate equations we solve for the edge region are as follows.

2.1 Density Equations: Hydrogenic

$$\frac{dN_1^+}{dt} = N_e N_o S_1 + N_e N_2^o S_3 + 2N_e N_2^o S_5 + N_e N_2^+ S_6 - N_p N_2^o S_8 - L_1^+ + \Gamma_1^+/\Delta \tag{1}$$

$$\frac{dN_2^+}{dt} = N_e N_2^o S_2 + N_p N_2^o S_8 - N_e N_2^+ S_6 - L_2^+ \tag{2}$$

$$\frac{dN_1^o}{dt} = - N_e N_o S_1 + N_e N_2^o S_3 + 2N_e N_2^o S_4 + N_e N_2^+ S_6 + N_p N_2^o S_8 + \Psi_1 L_1^+ + 2\Psi_2 L_2^+ \tag{3}$$

$$\frac{dN_2^o}{dt} = - N_e N_2^o S_2 - N_e N_2^o S_3 - N_e N_2^o S_4 - N_e N_2^o S_5 - N_p N_2^o S_8 + \frac{1}{2}\varphi_1 L_1^+ + \varphi_2 L_2^+ + \Sigma^2_{desorption} \tag{4}$$

$$N_e = N_p + N_2^+ + \sum_{k=2}^{9} (k-1)\, N_{o_k} \tag{5}$$

$$L_1^+ = \frac{N_p}{\tau} \qquad L_2^+ \equiv \frac{N_2^+}{\tau} \qquad \Gamma_1^+ = \text{plasma proton flux} \tag{6}$$

$\Psi_{1,2}$: Probability of H_2^o desorption by wall impact of H_1^+ and H_2^+, respectively. (See Glossary for other terms. The relevant rates (S) are described in Table I.)

3.2 Density Equations: Oxygen

$$\frac{1}{N_e}\frac{d}{dt}N_{O_k} = I_{k-1}N_{O_{k-1}} + R_{k+1}N_{O_{k+1}} - I_kN_{O_k} - R_kN_{O_k} - L_{O_k} \quad (9 \geq k \geq 2) \tag{7}$$

$$\frac{1}{N_e}\frac{d}{dt}N_{O_1} = R_2N_{O_2} - I_1N_{O_1} + \Sigma^{oxy}_{desorption} - L_{O_1} \tag{8}$$

L_{O_k} are the diffusive loss rates for oxygen. The specific models for $\Sigma^{2o}_{desorption}$ and $\Sigma^{oxy}_{desorption}$ will be discussed where they are relevant. I_k, R_k are the ionization and recombination rates.

3.3 Electron Energy Equation

$$\begin{aligned}\frac{d}{dt}\left[\frac{3}{2}N_eT_e\right] = {} & P_{core\ plasma} - N_eN_oS_1E_1 - N_eN_2^oS_2E_2 - N_eN_2^oS_3E_3 - N_eN_2^oS_4E_4 - N_eN_2^oS_5E_5 \\ & - N_eN_2^+S_6E_6 - N_eN_oS_{2x}(1.08\ E_{L\alpha}) \\ & - N_eN_oS_{3x}(0.65\ E_{L\beta} + 0.52\ E_{H\beta}) \\ & - N_eN_oS_{4x}(0.51\ E_{H\gamma} + 0.33\ E_{H\beta}) \\ & - 3\cdot 10^{-31}\ Z_{eff}\ N_e^2\sqrt{T_e} - 1.53\cdot 10^{-19}\ \frac{N_eN_p(T_e - T_p)\ln\Lambda}{A_MT_e^{3/2}} \\ & - 7.7\cdot 10^{-20}\ \frac{N_oN_2^+(T_e - T_2^+)\ln\Lambda}{A_MT_e^{3/2}} \\ & - \frac{3}{2}\frac{N_pT_e}{\tau} - \frac{3}{2}\frac{N_2^+T_e}{\tau} - N_eN_2^o(S_2+S_3+S_4+S_5)E_{XH_{20}} \\ & - P_{LINE} - P_{IONIZATION}\end{aligned} \tag{9}$$

where

$$P_{LINE} = \frac{45}{\sqrt{T_e}}N_e\left(\sum_{k=2}^{9} N_{o_k}C_k\, e^{-\epsilon_k/T_e} + \frac{1}{2}N_{O_6}\, e^{-83/T_e}\right)$$

$$\epsilon_k = (16,\ 18,\ 19,\ 20,\ 12,\ 575,\ 655)\quad k = 2,\ 8$$

$$C_k = (1,\ 1,\ 1.5,\ 1.25,\ 1.1,\ 1.25,\ .75)\quad k = 2,\ 8$$

$$Z_{eff} = \sum_{k=1}^{9}(k-1)^2\, N_{o_k}/N_e$$

3.4 Hydrogenic Energy Equations

$$\begin{aligned}\frac{d}{dt}\left[\frac{3}{2}N_1^+T_p\right] = {} & N_eN_2^oS_3\left(\frac{3/2\ T_2^o + \Delta E_3}{2}\right) + N_eN_2^oS_5\left(\Delta E_5 + \frac{3}{2}T_2^o\right) + N_eN_2^+S_6\left(\frac{3/2\ T_2^+ + \Delta E_6}{2}\right) \\ & + 1.53\ 10^{-14}\ N_eN_p(T_e - T_p)\ln\Lambda/A_MT_e^{3/2} + P_{core\ plasma} \\ & - 3.3\ 10^{-18}\ N_pN_2^+(T_p - T_2^+)\ln\Lambda/(T_p + T_2^+/2)^{3/2}\sqrt{A_M} \\ & - \frac{3}{2}N_pT_p/\tau + N_eN_1^oS_1\frac{3}{2}T_1^o - N_pN_1^oS_7\frac{3}{2}(T_p - T_1^o) - N_pN_2^oS_8\frac{3}{2}T_p\end{aligned} \tag{10}$$

$$\frac{d}{dt}\left(\frac{3}{2} N_2 T_2^+\right) = N_e N_2^o S_2 \left(\frac{3}{2} T_2^o\right) - N_e N_2^+ S_6 \left(\frac{3}{2} T_2^+\right) + N_p N_2^o S_8 \left(\frac{3}{2} T_2^o\right) + N_2^+ N_2^o S_4 \frac{3}{2} \left(T_2^o - T_2^+\right)$$
$$+ 7.7\ 10^{-20}\ N_e N_2^+ (T_e - T_2^+)\ \ln \Lambda / A_M T_e^{3/2}$$
$$+ 3.3\ 10^{-18}\ N_p N_2^+ (T_p - T_2^+) \ln \Lambda / \left(T_i + \frac{T_2^+}{2}\right)^{3/2} \sqrt{A_M} - \frac{3}{2} N_2^+ T_2^+ / \tau \qquad (11)$$

$$\frac{d}{dt}\left(\frac{3}{2} N_1^o T_1^o\right) = - N_e N_o S_1 \left(\frac{3}{2} T_1^o\right) + N_e N_2 S_3 \left(\frac{3}{2} T_2^o + \Delta E_3\right)/2$$
$$+ N_e N_2^o S_4 \left(\frac{3}{2} T_2^o + \Delta E_4\right) + N_e N_2^+ S_6 \left(\frac{3}{2} T_2^+ + \Delta E_6\right)/2$$
$$+ N_p N_o S_7 \frac{3}{2}\left(T_p - T_1^o\right) + N_p N_2^o S_8 \left(\frac{3}{2} T_i\right) + \Psi_1 \frac{N_p}{\tau} \left(\frac{3}{2} T_W\right)$$
$$+ 2\Psi_2 \frac{N_2^+}{\tau} \left(\frac{3}{2} T_W\right) - \frac{3}{2} N_o T_1^o (1 - R_E)/\tau_W \qquad (12)$$

$$\frac{d}{dt}\left(\frac{3N_2^o}{2} T_2^o\right) = - \frac{3}{2} T_2^o [N_e N_2^o (S_2 + S_3 + S_4 + S_5) + N_p N_2^o S_8]$$
$$+ N_2^+ N_2^o S_9 \frac{3}{2}\left(T_2^+ - T_2^o\right) + \frac{N_p}{\tau} \frac{1}{4} T_W + \Psi_2 \frac{N_2^+}{\tau} \frac{3}{2} T_W - \frac{3}{2} N_2^o T_2^o (1 - R_E)/\tau_W \qquad (13)$$

The reaction rates S_1 through S_9 and S_{2x}, S_{3x}, S_{4x} are listed in Table I. These include processes for ionization, excitation, dissociation, and charge exchange. The L_{1+} and L_{2+} are particle loss rate terms which also carry an energy loss. The confinement time is taken to be Bohm or Pfirsch-Schlüter (whichever is shorter) for the scrape-off plasma. The protons diffusing to the wall recombine to return as H_1^o with probability Ψ_1 and as H_2^o with probability φ_1. Similarly, the H_2^+ ions diffusing to the wall recombine as H_1^o with probability Ψ_2 and as H_2^o with probability φ_2.

We assume that the oxygen equilibrates fast enough so that the proton and oxygen ion temperatures are equal. This eliminates the need for a separate oxygen energy equation.

These equations are calculated in the following way. An initial value is given to begin. The radial transport model computes the appropriate fluxes and the boundary calculation is then moved along from t to t + Δt. These boundary values are then used to compute the radial transport for the next timestep.

Figure 2 shows a typical calculated time evolution of the computed boundary quantities. We assume a desorption yield ~ 0.005 atoms/photon for 100 kW of 1032 Å radiation (OVI). The calculation neglects all other processes, and starts at t = 0. As oxygen is evolved from the surface, the electron density rises and temperatures drop to a few eV.

3. IMPURITY TRANSPORT MODELS

We may first discuss the transport of impurities by decoupling the production processes from the calculation. For present experiments there are laser Thomson scattering measurements which allow reasonable estimates of densities and temperatures near the edge. Also, the neutral transport physics is sufficiently straightforward that, with a proper cylindrical model such as XSDRN[8], one may calculate the edge neutral density once the central charge exchange flux is known. (This latter technique is valid, of course, only when the discharge is known to be dominated by a single low-Z species, such as oxygen, for which some quantitative estimate of the proton density is possible.)

Thus, we will treat impurity transport processes in this section by applying the usual edge conditions and using experimental estimates for the neutral and impurity influxes. We will discuss two cases: diffusion of iron ('high Z') and oxygen ('low Z').

3.1 Diffusion of Iron

We will discuss simple neoclassical transport of a 'high-Z' impurity (iron in our case) to investigate the magnitude of anomalous spreading which should be added to the neoclassical impurity diffusion equations to match the experimental results.

The impurity transport model is discussed in the Appendix. As an edge condition we will assume that there is no sputtering of the wall by charge exchange neutrals. Further we will study the plateau phase of discharge, reported by the TFR group[6], assuming that there are 2×10^{10} cm^{-3} of iron atoms present initially, distributed uniformly in radius. We take an initial central density of 3.5×10^{13} cm^{-3} and a fixed boundary density of 10^{13} cm^{-3}.

Figure 3 shows the evolution in time of n_{Fe}. Although the rise of $n_{Fe}(0)$ in time is substantial, this effect is due solely to rearrangement of the assumed initial 2×10^{10} cm^{-3} density; N_{Fe} (the total number of iron atoms) is constant (we have assumed that there is no sputtering). The rise in central density is not evidence of sputtering by itself, since the neoclassical diffusion process pushes the original number of impurities into a small volume, thus substantially increasing the number density without increasing the number.

Figure 4 shows the time evolution of $n_{Fe}(0)$, $Z^{Fe}_{eff}(0)$ and N_{Fe} for various values of α, where the anomalous spreading diffusion coefficient is taken to be αD_p. Choosing $\alpha \sim 0.3$ will reproduce the observations.

3.2 Diffusion of Oxygen

We examine the same case, but now using only oxygen. The flow rate $\Psi^0 \sim 2 \times 10^{15}$ cm^{-2} s^{-1} reported in [6] is assumed for inflowing oxygen at the edge. Figure 5 (a-d) shows the evolution of T_e, j_z, q, oxygen density profiles as a function of time. We note that, as new oxygen flows in, the radiative losses cause a strong contraction of the current channel. The edge T_e drops and, because of the resulting increase in resistivity, so does the current density. Since the total current is programmed to be constant in the plateau phase of the experiment, the current density must increase elsewhere in the volume. The magnetic diffusion time is a maximum on axis, and so the behavior shown in Fig. 5 is the result: there results an off-axis peak in $j_z(r)$. The q(r) profile shows a local minimum, and so the plasma is susceptible to a wide variety hydromagnetic instabilities.

This implies that our radial transport model cannot supply an accurate description: fast time scale MHD processes will surely flatten the j_z profile and produce a broad shear-free central q(r) profile.

The effect of this mixing process will be to produce a steady-state in the impurity balance. The turbulent mixing will produce the efflux of fully stripped oxygen atoms which is needed to balance the incoming lower ionized states. We note that $q(0) > 1$. Thus the conditions of low shear which are provided by the high impurity influx can be present for high q(a). It follows that the narrowing of stability boundaries against strong disruption should be very sensitive to the state of cleanliness of the wall in this model as it is observed to be in practice.

APPENDIX

Particle Balance: We treat the electron balance, using charge neutrality to determine the proton density.

$$\frac{\partial}{\partial t} N_e(r,t) + \frac{1}{r}\frac{\partial}{\partial r}(rN_eV) = N_eN_o\langle\sigma v\rangle_{ion} + \Sigma_{IMP} + \Sigma_{BEAM} \equiv R + \Sigma_{BEAM} \tag{1}$$

Electron Energy Balance:

$$\frac{3}{2}\frac{\partial}{\partial t}(N_eT_e) = \frac{1}{r}\frac{\partial}{\partial r}[r(q_e + \frac{3}{2}N_eVT_e)] - 3\frac{m_e}{m_p}\frac{T_e - T_p}{\tau_e} + E\,j + R\,T_o - P_{rad} + Q^e_{Inj} \tag{2}$$

The electron energy balance treats the conduction (q_e), convection ($\frac{3}{2}N_eVT_e$), electron-proton thermal equilibration, ohmic heating, the source of cold electrons, radiative losses and auxiliary heating. The calculations for q_e, V, E, j, P_{Rad}, and Q^e_{Inj} are discussed, for example, by Hogan[3].

Proton Energy Balance:

$$\frac{3}{2}\frac{\partial}{\partial t}(N_pT_p) = -\frac{1}{r}\frac{\partial}{\partial r}[r(q_p + \frac{3}{2}N_eVT_p)] + 3\frac{m_e}{m_p}\frac{T_e - T_p}{\tau_e} - N_pN_o\langle\sigma v\rangle_{CX}(T_p - T_o)$$
$$+ Q^P_{Inj} + RT_o \tag{3}$$

Field Diffusion: The relevant electromagnetic equations and an Ohm's law

$$\frac{\partial B}{\partial t} = \frac{\partial E}{\partial r}\ ;\ \mu_o j = \frac{1}{r}\frac{\partial}{\partial r}$$
$$j = E/\eta + j_B \tag{4}$$

GLOSSARY OF TERMS

$N_{e,p}$: Electron, proton density

V: Ambipolar diffusion velocity (defined below)

N_o: Density of neutrals

$\langle\sigma v\rangle_{ion}$: Rate of electron impact ionization of neutral H

Σ_{IMP}: Source of electrons from impurity stripping

Σ_{BEAM}: Source of electrons from injected beam

A $T_{e,p}$: Electron, proton temperature

$q_{e,p}$: Electron-proton heat flux

$m_{e,p}$: Electron, proton masses

τ_e: Electron-ion scattering time, $= 3\sqrt{m_e}T_e^{3/2}/4\sqrt{2\pi}\,\lambda e^4 N_p$

(λ = Coulomb logarithm, e: electron charge)

E: Longitudinal electric field

j: Longitudinal current density

T_o: Mean energy of H_o

P_{Rad}: Losses due to all forms of radiation: bremsstrahlung, recombination and line radiation

$Q^{e,p}_{Inj}$: Energy source from injection for electrons, protons

$\langle\sigma v\rangle_{CX}$: Charge exchange rate

B: Poloidal magnetic field

η: Plasma resistivity

j_B: Beam-induced current

N^o_2, N^+_2: Density of H^o_2, H^+_2

T^o_2, T^+_2, T^o_1: Mean energy of H^o_2, H^+_2, H^o_1

TABLE I

Densities Reaction	Energy	Input	Output	Gain	Loss
$N_e N_1^o S_1$	E_1	$e + H_1^o$	$e + H_1^+ + e$	H_1^+	H_1^o
$N_e N_2^o S_2$	E_2	$e + H_2^o$	$e + H_2^+ + e$	H_2^+	H_2^o
$N_2^o S_3$	E_3	$e + H_2^o$	$e + H_1^+ + H_1^o + e$	$H_1^+ + H_1^o$	H_2^o
$N_e N_2^o S_4$	E_4	$e + H_2^o$	$e + H_1^o + H_1^o$	$2H_1^o$	H_2^o
$N_e N_2^o S_5$	E_5	$e + H_2^o$	$e + H_1^+ + H_1^+ + e + e$	$2H_1^+$	H_2^o
$N_e N_2^+ S_6$	E_6	$e + H_2^+$	$e + H_1^+ + H_1^o$	$H^+ + H_1^o$	H_2^+
$N_1^+ + N_1^o S_7$	E_7	$H_1^+ + H_1^o$	$H_1^o + H_1^+$	---	---
$N_1^o + N_2^o S_8$	E_8	$H_2^+ + H_2^o$	$H_2^o + H_2^+$	$H_1^o + H_2^+$	$H_1^+ + H_2^o$
S_9	E_9	$H_2^+ + H_2^o$	$H_2^o + H_2^+$	---	---
$L_{H_1^+}$		$L_{H_1^+}$	$H_1^o \quad H_2^o$	$\Psi_1 L_{H_1^+} \quad \frac{\varphi_1}{2} L_{H_1^+}$ $H_1^o \quad H_2^o$	H_1^+
$L_{H_2^+}$		$L_{H_2^+}$	$H_1^o \quad H_2^o$	$2\Psi_2 L_{H_2^+} \quad \varphi_2 L_{H_2^+}$ $H_1^o \quad H_2^o$	H_2^+
$N_e N_1^o S_{2x}$		$e + H_1^o(n=1)$	$e + H_1^o(n=2)$		
$N_e N_1^o S_{3x}$		$e + H_1^o(n=1)$	$e + H_1^o(n=3)$		
$N_e N_1^o S_{4x}$		$e + H_1^o(n=1)$	$e + H_1^o(n=4)$		

REFERENCES

[1] MERCIER, C. and SOUBBARAMAYE[illegible] Numerical Models for P[illegible] a Evolution in Tokamak Devices," Fifth European Con[illegible]ce on Controlled Fusi[illegible] Plasma Physics, Grenoble, 1972.

[2] DUCHS, D. F. FURTH, H. P., an[illegible] UTHERFORD, P. H., "Nu[illegible]al Calculations of the Radial Transport in Tokamak Dischar[illegible]," Proceedings of the T[illegible] International Symposium on Toroidal Confinement," Garchi[illegible], 1973.

[3] HOGAN, J. T., "Multifluid Tok[illegible] Transport Models," M[illegible]ds of Computational Physics, V. 16, Computer Applications [illegible] Controlled Fusion Rese[illegible], Academic Press (in press).

[4] HOTSON, E., and MCCRACKEN, G. [illegible], "Investigation of Pla[illegible] Recycling at Surfaces Using a Self-Consistent Model for t[illegible] Plasma-Wall Interactio[illegible]," J. Nucl. Mater. (to appear).

[5] HINNOV, E., BISHOP, A. S., an[illegible] ALLON, H., Jr., "Comput[illegible] Description of the C-Stellerator Ohmic Heating Dis[illegible]ges in Hydrogen," Plas[illegible] Physics 10:291 (1968), also MARCUS, F. B. and ATTENBERGER, [illegible] E., "Tokamak Startup [illegible]e," private communication.

[6] TFR Group, "Line Radiation in the Visible and Ultraviol[illegible] in TFR Tokamak Plasmas," Nucl. Fus. 15:1053 (1975).

[7] MIRNOV, S. V and SEMENOV, I. [illegible], "Observation of the P[illegible] Structure of a Disruptive Instability in a Tokamak Devic[illegible]," Sixth IAEA Conference [illegible] Plasma Physics and Controlled Nuclear Fusion, Berchtesgaden, 1976.

[8] CRUME, E. C., et al., "The NU[illegible]N Code," private commu[illegible]ation and ENGLE, W. W., Jr., "A User's Manual for ANISN," O[illegible] Ridge AEC R and D Repo[illegible] K-1693, 1966.

[9] RUTHERFORD, P. H., "Impurity D[illegible]fusion in the Pfirsch-S[illegible]üter Regime," Phys. Fluids 17:1782 (1974) and MOORE, T. B. and HINTON, F. L., "Impu[illegible]ty Transport in the Banana-Plateau Regime," Nucl. Fus. 14:[illegible]39 (1974).

FIGURE CAPTIONS

Fig. 1 A generalized view of the geometry. Processes occurring in the volume V_S are treated by the zero-dimensional code. The only spatial attributes of V_S are the mean thickness Δ, defined as the ratio of V_S to the plasma surface area, and the ratio of the wall area to the plasma surface area. This latter quantity is not used in the paper, but it is important to studies both of the effects of bellows configurations and of gettering.

Fig. 2 Typical result for an ORMAK case. The evolution of H_o and oxygen at the wall is stimulated by a hypothesized photoelectron desorption due to line radiation.

Fig. 3 Pure neoclassical evolution of the iron density for a TFR case. The $\langle z \rangle$ of ions is shown at the top, while the spatial evolution of N_{Fe} appears at the bottom. The neoclassical peaking leads to a sharp rise in central density without an increase in the total number of iron atoms.

Fig. 4 The effects are shown of adding in the particle diffusion D as an 'anomalous spreading' in the impurity diffusion. The result of Fig. 3 is reproduced for $\alpha = 0$, while $\alpha = 0.5$ produces levels more nearly in accord with observation.

Fig. 5 Evolution of the discharge with an oxygen flux $\Gamma_{oxy} \sim 2 \cdot 10^{15}\ cm^{-2}\ s^{-1}$ at the boundary. A flux of this magnitude causes the off-axis peak in j_z (top left) which produces a local minimum in q (top right). The T_e profile peaks in the center (lower left) while the oxygen level is controlled by the slow response of N_e (lower left).

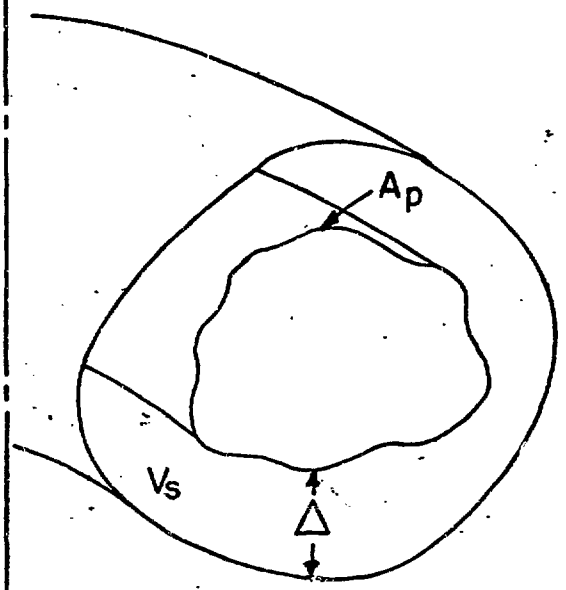

GEOMETRY

$$\Delta \equiv V_s / A_p$$

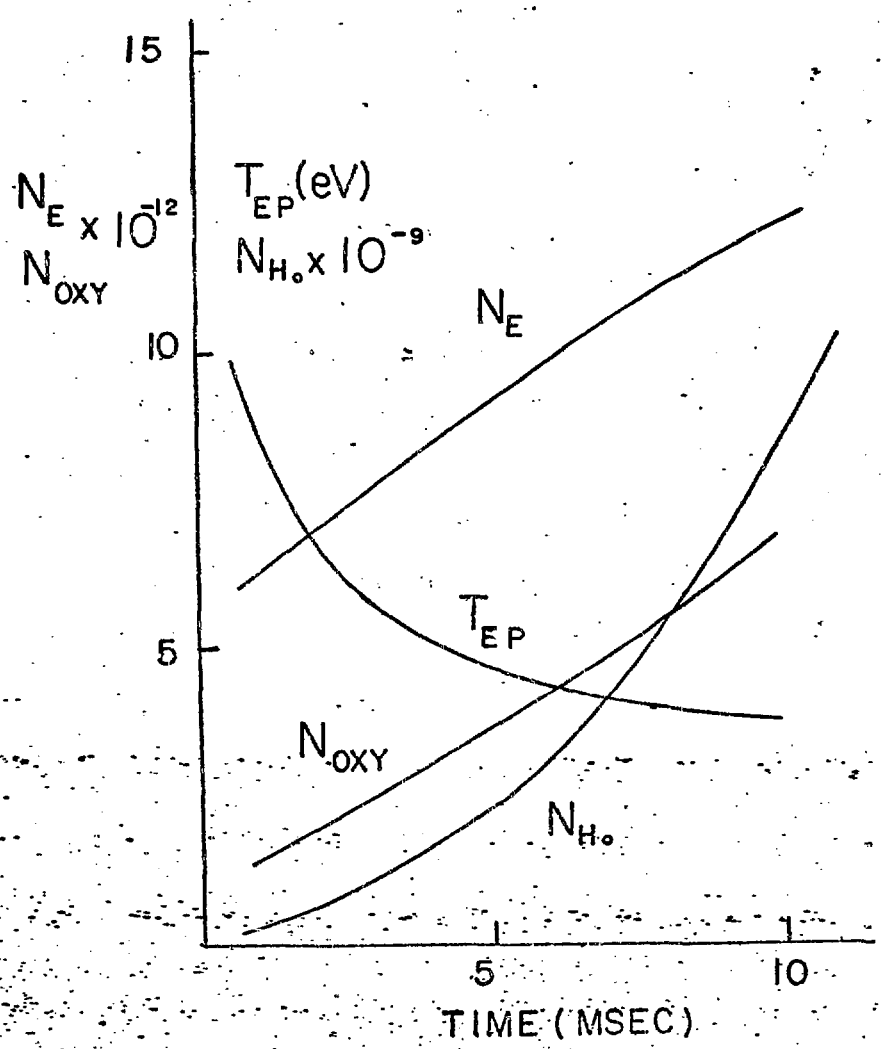
15
10
5
$N_E \times 10^{-12}$
N_{OXY}
T_{EP}(eV)
$N_{H_o} \times 10^{-9}$
N_E
T_{EP}
N_{OXY}
N_{H_o}
5
10
TIME (MSEC)

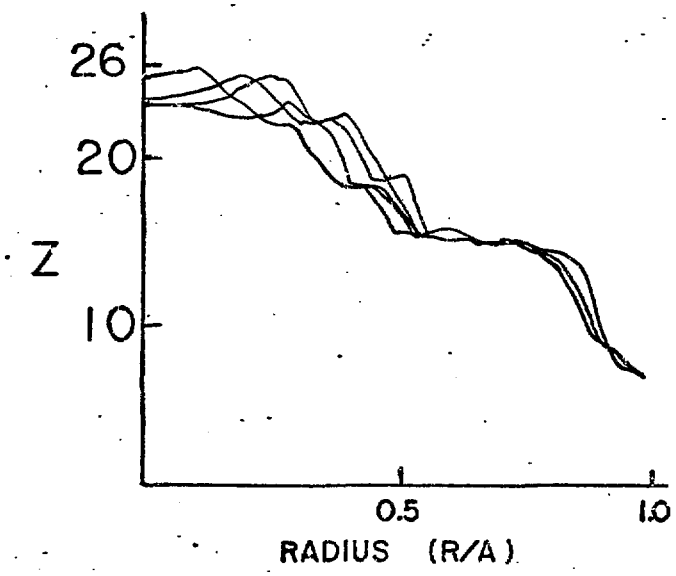
26
20
Z
10
0.5
1.0
RADIUS (R/A)

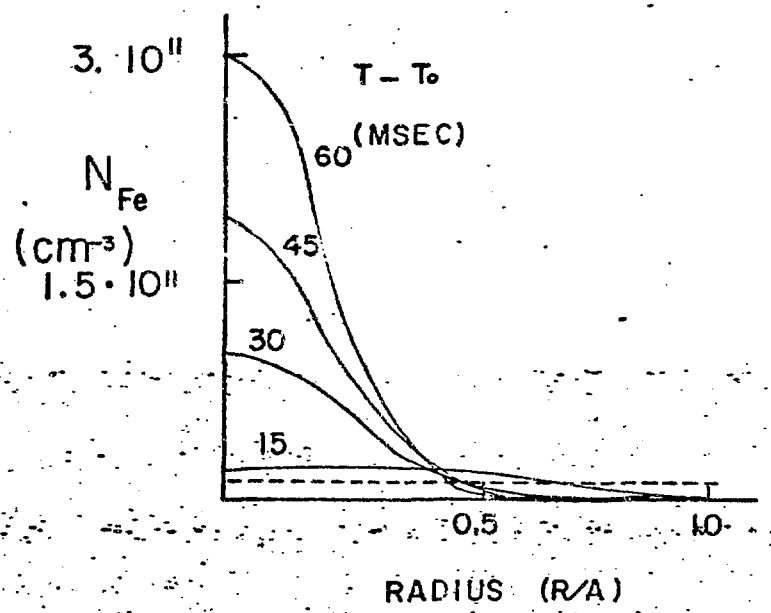
3. 10¹¹
T – T₀
(MSEC)
60
N_Fe
(cm⁻³)
45
1.5 · 10¹¹
30
15
0.5
1.0
RADIUS (R/A)

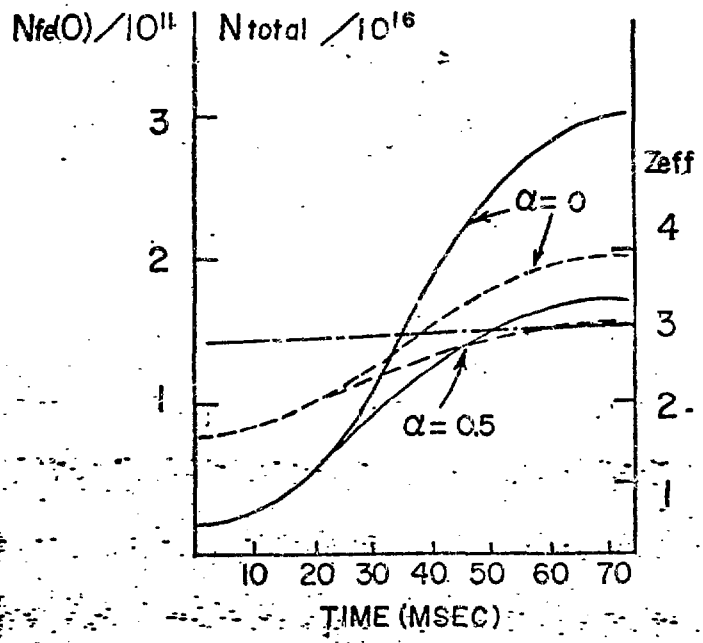

$$\frac{N_{Fe}(O)}{Z_{Eff}(O)\,N_{total}}$$

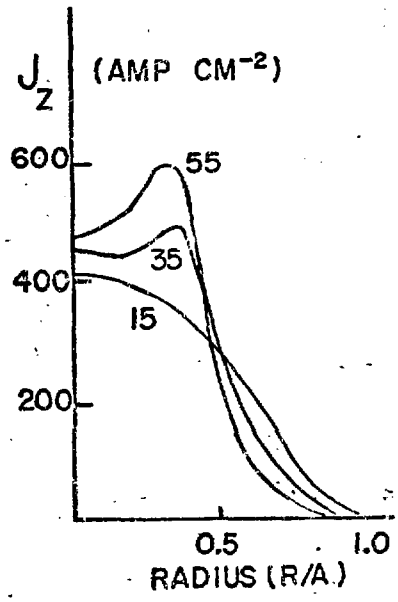
J_Z (AMP CM^{-2})
600
400
200
55
35
15
0.5
1.0
RADIUS (R/A)

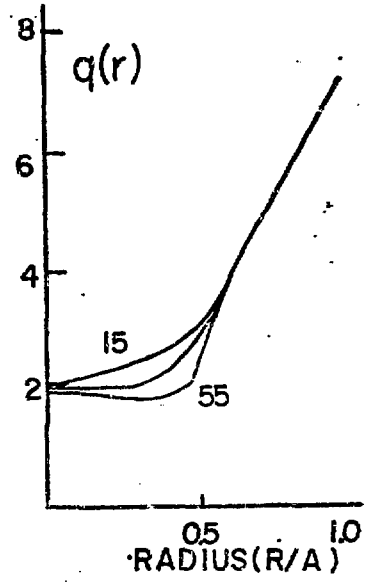
q(r)
8
6
4
2
15
55
0.5
1.0
RADIUS(R/A)

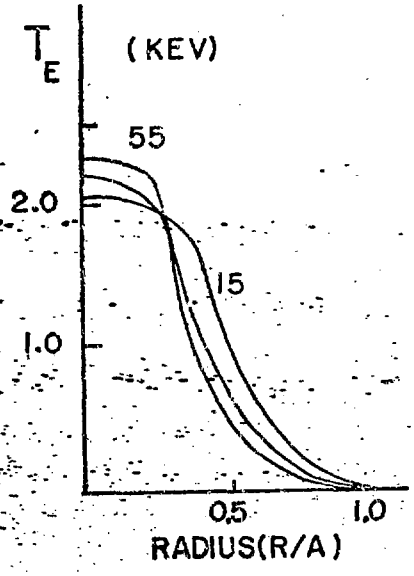
T_E (KEV)
55
2.0
15
1.0
0.5
1.0
RADIUS(R/A)

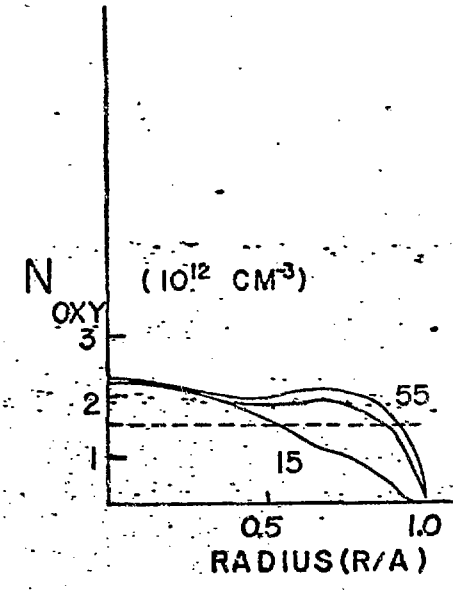
N_{OXY} (10^{12} CM^{-3})
3
2
1
55
15
0.5
1.0
RADIUS(R/A)